Gasotransmitters Hot Paper

How to cite: *Angew. Chem. Int. Ed.* **2023,** *62,* e202302303
International Edition: doi.org/10.1002/anie.202302303
German Edition: doi.org/10.1002/ange.202302303

Enzyme-Triggered Chemodynamic Therapy via a Peptide-H_2S Donor Conjugate with Complexed Fe^{2+}

Yumeng Zhu, William R. Archer, Katlyn F. Morales, Michael D. Schulz, Yin Wang, and John B. Matson**

Abstract: Inducing high levels of reactive oxygen species (ROS) inside tumor cells is a cancer therapy method termed chemodynamic therapy (CDT). Relying on delivery of Fenton reaction promoters such as Fe^{2+}, CDT takes advantage of overproduced ROS in the tumor microenvironment. We developed a peptide-H_2S donor conjugate, complexed with Fe^{2+}, termed **AAN-PTC–Fe^{2+}**. The AAN tripeptide was specifically cleaved by legumain, an enzyme overexpressed in glioma cells, to release carbonyl sulfide (COS). Hydrolysis of COS by carbonic anhydrase formed H_2S, an inhibitor of catalase, an enzyme that detoxifies H_2O_2. Fe^{2+} and H_2S together increased intracellular ROS levels and decreased viability in C6 glioma cells compared with controls lacking either Fe^{2+}, the AAN sequence, or the ability to generate H_2S. **AAN-PTC–Fe^{2+}** performed better than temezolimide while exhibiting no cytotoxicity toward H9C2 cardiomyocytes. This study provides an H_2S-amplified, enzyme-responsive platform for synergistic cancer treatment.

Introduction

Elevating intracellular levels of reactive oxygen species (ROS) can kill cancer cells with high specificity, with ROS-induced oxidative damage to lipids, DNA, and proteins.[1] Chemodynamic therapy, a method of treating tumors developed in 2016 by Bu, Shi, and co-workers, takes advantage of ROS-induced cytotoxicity by relying on the higher levels of ROS in the tumor microenvironment (TME) compared with the normal tissue environment.[2] A common CDT design utilizes the reaction of metal salts (e.g., Fe^{2+}) with overproduced H_2O_2 in the TME to favor production of highly cytotoxic hydroxyl radicals ($^{\bullet}OH$) by the Fenton reaction ($Fe^{2+} + H_2O_2 \rightarrow Fe^{3+} + {}^{\bullet}OH + OH^-$).[3,4] Despite the potential selectivity and precise targeting of this new tumor treatment method, its efficacy is inherently limited by H_2O_2 levels.[5] A potential solution to break this bottleneck is to inhibit catalase (CAT), one of the major antioxidant enzymes in cells that catalyzes the decomposition of H_2O_2 into water and oxygen.[6]

A recently identified inhibitor of CAT is the signaling gas (gasotransmitter) hydrogen sulfide (H_2S).[7–11] First established as a gasotransmitter in 1996,[12] H_2S carries out a wide variety of signaling functions across many cell types. Exogenous H_2S delivery has been examined in the context of cancer with mixed results, where it increases cancer cell proliferation under certain conditions and limits growth under others.[13,14] Precise delivery of H_2S to cancer cells therefore might improve CDT outcomes in cancer treatments. Thus, we hypothesized that H_2S in combination with a Fenton reaction promoter like Fe^{2+} could be an effective way to selectively kill tumor cells.

Glioma is a particularly difficult cancer that has limited success with surgery and chemotherapy, and a low survival rate. Gliomas derive from glial cells and occur in the brain and spinal cord, and they are one of the most common types of primary brain tumors.[15] Gliomas are known for their high proliferation and growth rates, and glioma patients have a poor prognosis with a 5-year survival rate of only 7%.[16] While new glioma targets and new lead compounds have been developed in recent years,[17–23] a simple, efficient, and precise platform for glioma treatment remains a major goal in cancer therapy. Interestingly, legumain, a lysosomal cysteine protease that exclusively cleaves the C-terminus of the Ala-Ala-Asn (AAN) peptide sequence, is overexpressed in several types of primary human tumor cells, including glioma cells,[24] making it a potential target to promote CDT.[25]

Here we investigate the combination of a Fenton reaction promoter (Fe^{2+}), with a CAT inhibitor (H_2S), as a CDT method initiated by legumain. Ferrous sulfide (FeS) has been evaluated as a donor for Fe^{2+} and H_2S;[11] however, this platform could neither precisely target cancer cells nor

[*] Y. Zhu, W. R. Archer, K. F. Morales, M. D. Schulz, Y. Wang, J. B. Matson
Department of Chemistry,
Virginia Tech Center for Drug Discovery, and Macromolecules Innovation Institute,
Virginia Tech
24061 Blacksburg, VA (USA)
E-mail: jbmatson@vt.edu

Y. Wang
Engineering Research Center of Cell & Therapeutic Antibody,
School of Pharmacy,
Shanghai Jiao Tong University
200240 Shanghai (China)
E-mail: yinwang@sjtu.edu.cn

release H_2S gas at a controlled rate, which is critical for effective delivery. Therefore, we designed a novel peptide–H_2S donor conjugate (PHDC) that we anticipated would degrade in the presence of legumain to generate carbonyl sulfide (COS), which could be quickly converted into H_2S by the ubiquitous enzyme carbonic anhydrase (CA). By combining this PHDC with Fe^{2+}, we hypothesized that this unique PHDC–Fe^{2+} complex would merge the benefits from H_2S and a Fenton reaction promoter, providing a precise platform that targets gliomas, thus selectively killing tumor cells (Figure 1).

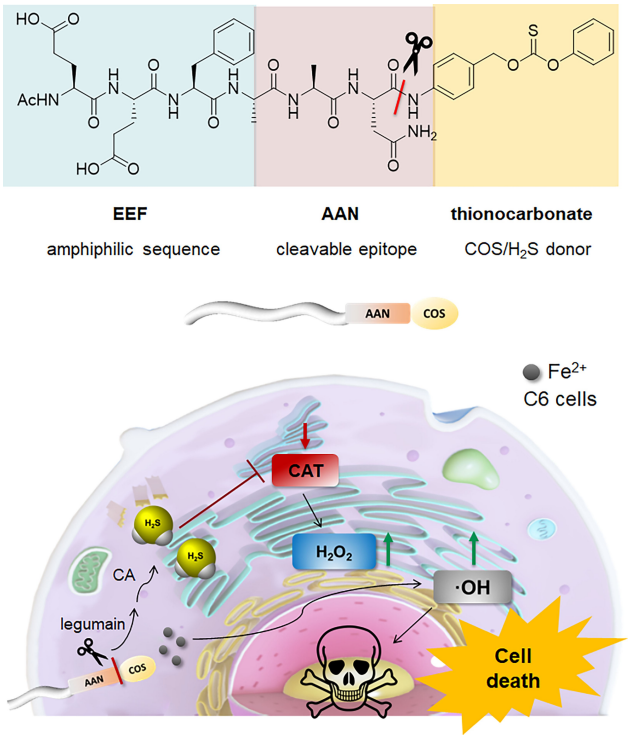

Figure 1. Schematic illustration of PHDC-Fe^{2+} complex chemical structure and therapeutic mechanism in C6 glioma cell line.

Results and Discussion

PHDC Design and Synthesis

A wide variety of H_2S donors have been designed over the past decade,[26–29] with several generating COS and relying on its CA-mediated conversion into H_2S.[30–33] Here we designed and synthesized a legumain-responsive, COS-releasing PHDC termed **AAN-PTC** (Scheme 1; AAN represents the peptide component, and PTC represents the phenyl thionocarbonate). The peptide component included the hexapeptide Ac-Glu-Glu-Phe-Ala-Ala-Asn (**EEFAAN**, Figure S1), where the EEF segment provided amphiphilicity and the AAN segment was the legumain-responsive epitope. We synthesized the peptide on chlorotrityl resin so that it could be cleaved while retaining the side chain protecting groups (Scheme S1). To introduce the H_2S donor onto the cleaved but still protected peptide, we then added 4-amino-benzyl alcohol (4AB) to the C-terminus via amidation using *N*-ethoxycarbonyl-2-ethoxy-1,2-dihydroquinoline (EEDQ) to form **EEFAAN-4AB** (Figure S4). Phenyl chlorothionoformate was then added to **EEFAAN-4AB** to produce the desired benzyl phenyl thionocarbonate linkage. Global deprotection using trifluoroacetic acid (TFA) afforded the final PHDC, termed **AAN-PTC**. We envisioned that legumain, which cleaves the amide bond on the C-terminal side of the AAN sequence, would trigger a 1,6-elimination to release COS, which would be rapidly hydrolyzed into H_2S via the action of the ubiquitous enzyme CA.[34,35]

To test both the legumain specificity and the effect of H_2S in cell studies, we also synthesized two control peptides. First, to determine the specificity of the sequence for legumain, we replaced the Asn residue with a Gln residue to generate PHDC **AAQ-PTC**. We envisioned that this PHDC would serve as a control that varied structurally from **AAN-PTC** by a single methylene unit but should be unable to release COS/H_2S (Figure 2A). In the second control peptide, we replaced the phenyl thionocarbonate with a phenyl carbonate. We envisioned that this control PHDC, termed

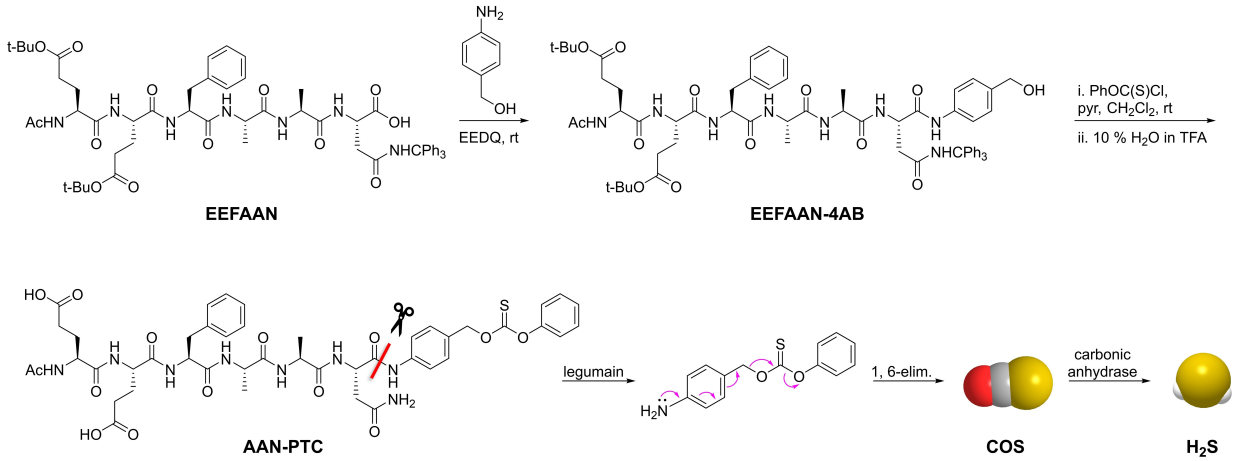

Scheme 1. Synthetic route to **AAN-PTC** and COS/H_2S release triggered by legumain and aided by CA. A detailed synthetic route to **AAN-PTC** appears in the Supporting Information.

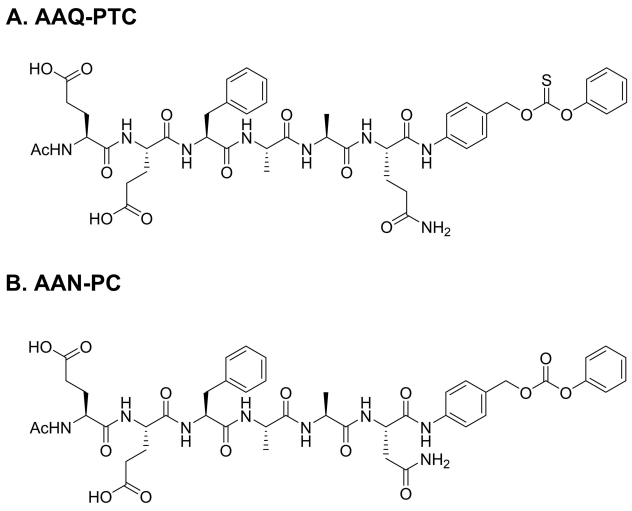

Figure 2. Chemical structures of control PHDCs: A) **AAQ-PTC**, which does not respond to legumain, and thus cannot release H_2S. B) **AAN-PC**, which responds to legumain but releases CO_2 instead of COS, and thus cannot generate H_2S.

AAN-PC, should still undergo cleavage in response to legumain but would release CO_2 rather than COS and would thus not generate H_2S (Figure 2B). Both retained the solubilizing EEF component. We made these PHDCs using routes similar to that for **AAN-PTC** (Figure S6–S8).

H_2S Release

To study whether **AAN-PTC** could be degraded by legumain, we first examined its enzymatic degradation by mass spectrometry. We collected solutions after enzyme treatment for 4 h and examined them using matrix-assisted laser desorption/ionization time of flight (MALDI-TOF) mass spectrometry. For **AAN-PTC** with legumain and CA, a clear peak representing the hexameric peptide after enzymatic removal of the phenyl thionocarbonate ($m/z = 722$) appeared, as well as a peak representing the original PHDC **AAN-PTC** ($m/z = 963$) (Figure S9A). In contrast, PHDC **AAQ-PTC** showed a major peak corresponding to the original PHDC **AAQ-PTC** ($m/z = 977$) (Figure S9B) with only a small peak representing the peptide after enzymatic degradation ($m/z = 736$), suggesting slow degradation of the AAQ sequence by legumain. Finally, after enzymatic degradation of **AAN-PC** by legumain, there was a clear peak representing the same hexameric peptide as derived from **AAN-PTC** ($m/z = 722$) (Figure S9C), which suggested that legumain recognized AAN and cleaved the sequence in this control PHDC as well.

After confirming that legumain degraded **AAN-PTC**, we then used an H_2S-selective microelectrode probe with a custom-made vial that has been previously used in our lab to evaluate H_2S release (Figure S10).[36] In each experiment, CA along with **AAN-PTC** or a control PHDC solution, with or without legumain, was loaded into the inner well of the vial. All studies were conducted in pH 5.0 acetate buffer because mildly acidic conditions activate legumain.[37] The inner well was then sealed with a gas-permeable membrane, and the vial was filled with buffer, allowing H_2S generated in the inner well to permeate to the outside buffer solution. The concentration of H_2S was monitored by the electrochemical probe over time (Figure 3A). The dual enzyme-responsive PHDC **AAN-PTC**, which underwent cleavage by legumain followed by CA-mediated hydrolysis of COS, demonstrated sustained H_2S release with a peaking time at 65 ± 4 min. Due to the well-in-vial design used for these experiments, the peaking concentration appeared much lower than the actual H_2S release levels. We determined total H_2S released using a different assay discussed below. With no recognizable cleavage site for legumain, the control PHDC **AAQ-PTC** showed very slow H_2S release at levels at least 10-fold lower than the amount released from **AAN-PTC** over this time period. The small H_2S release from **AAQ-PTC** is likely a result of much slower recognition by legumain of this sequence. In sharp contrast, the other control PHDC **AAN-PC** showed no H_2S release due to the lack of a COS donor. We then compared the H_2S release profiles of PHDC only, PHDC with legumain only, and PHDC with CA only. We observed very low or no release at all under each of these conditions (Figure S11), indicating the necessity of both enzymes (legumain and CA) to trigger H_2S release.

While the electrochemical probe provides a real-time analysis of H_2S release, this method cannot accurately

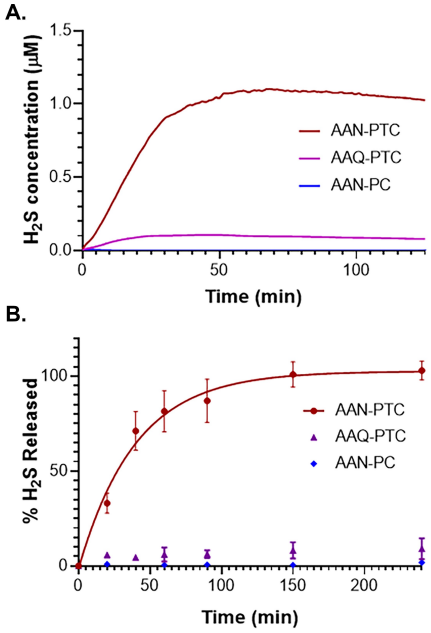

Figure 3. A) Representative H_2S release profiles of **AAN-PTC**, **AAQ-PTC**, and **AAN-PC** (333 μM) triggered by CA (3.33 μM) and legumain (1 ng μL^{-1}) at rt in acetate buffer (10 mM, pH 5.0). Data were obtained on an H_2S-sensitive electrochemical probe. B) H_2S release kinetics from **AAN-PTC**, **AAQ-PTC**, and **AAN-PC** (100 μM) measured via the methylene blue assay in acetate buffer (10 mM, pH 5.0) with CA (1 μM) and legumain (1 ng μL^{-1}). Data points are solid circles, and the solid line shows the pseudo-first-order kinetics fit for **AAN-PTC**. Error bars indicate standard deviations of three separate experiments.

determine the half-life of H_2S release because the released H_2S must penetrate the gas-permeable membrane to reach the buffer solution, where it can oxidize and volatilize before it interacts with the microelectrode probe. Thus, we used the methylene blue assay with a simpler reaction setup to measure and compare H_2S release of these three PHDCs. In these experiments, PHDCs in acetate buffer at pH 5.0 were mixed with CA, legumain, and $Zn(OAc)_2$ to capture the H_2S as ZnS. At predetermined timepoints, aliquots were taken from each vial and diluted with equal volumes of $FeCl_3$ and *N*,*N*-dimethyl-*p*-phenylenediamine dihydrochloride solution to form methylene blue. After incubating for at least 8 h, the absorbance for each aliquot was measured at 750 nm. As shown in Figure 3B, the half-life ($t_{1/2}$) of **AAN-PTC** was 29 ± 4 min, similar to the timescale of release in the electrochemical probe experiments, and the total H_2S release amount was 26 μM (Figure S12A,B). Control PHDC **AAQ-PTC** showed too little H_2S release to determine a half-life, and PHDC **AAN-PC** showed no measurable release (Figure S12B). The methylene blue studies revealed a ≈15-fold difference in release amount between **AAN-PTC** and **AAQ-PTC**, consistent with the electrochemical probe results.

In Vitro H_2S Release from PHDCs

We explored the ability of PHDCs **AAN-PTC**, **AAQ-PTC**, and **AAN-PC** to release H_2S in vitro using fluorescence-based imaging. We chose glioma C6 cells, which overexpress legumain, and imaged them using fluorescence microscopy with an H_2S-responsive turn-on fluorescent probe to investigate whether **AAN-PTC** could deliver H_2S to the C6 cells. WSP-5 is an H_2S-selective fluorescent probe,[38] which we used to visually monitor the delivery and accumulation of H_2S from the PHDCs to the cells. In these experiments, C6 cells were pre-treated with WSP-5 for 30 min before removing excess WSP-5 and incubating for 3 h with **AAN-PTC**, **AAQ-PTC**, **AAN-PC**, or H_2S as a positive control. All wells were then imaged to visualize H_2S accumulation within the cells.

The results showed that the blank group, i.e., those that received WSP-5 but no other treatment, had low H_2S signal (Figure 4A, first row), consistent with low background levels of H_2S in C6 cells. The Na_2S group, as the positive control, showed a distinct green fluorescence signal throughout all of the cells (Figure 4A, second row). **AAN-PTC** provided a strong fluorescent signal, similar in intensity to Na_2S (Figure 4A, third row). This result suggested that **AAN-PTC** can be successfully and efficiently cleaved by the overexpressed legumain in C6 cells, releasing H_2S in vitro. A weak fluorescent signal was observed when treating cells with **AAQ-PTC** (Figure 4A, fourth row), consistent with the mass spectrometry results as well as the H_2S release studies, indicating slow cleavage of the AAQ unit. In sharp contrast, **AAN-PC** showed H_2S levels similar to the untreated control group because there was no H_2S donor in the structure (Figure 4A, fifth row). Average fluorescence intensities across several images from each group were quantified, with Na_2S and **AAN-PTC** showing similar fluorescence intensity,

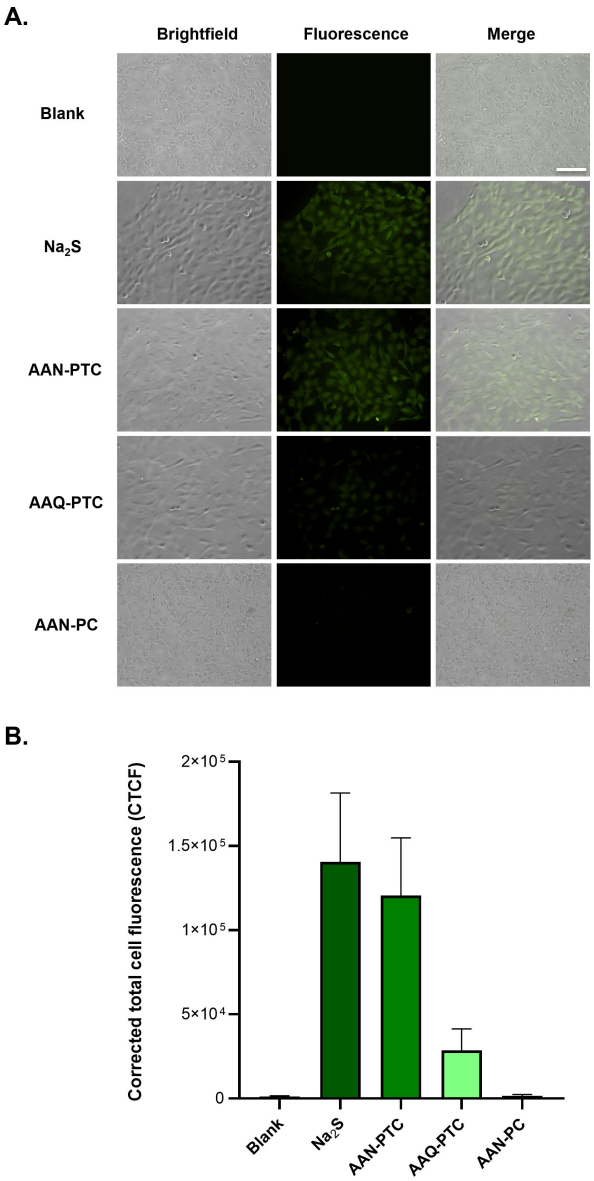

Figure 4. A) Brightfield, fluorescence, and merged images showing fluorescence in C6 cells preincubated with H_2S probe WSP-5 (50 μM) for 30 min and then treated with the following groups for 3 h: blank (PBS), Na_2S (200 μM), **AAN-PTC** (with cleavable site and H_2S donor, 200 μM), **AAQ-PTC** (with H_2S donor but no cleavable site, 200 μM), **AAN-PC** (with cleavable site but no H_2S donor, 200 μM). Cells were then washed, and fluorescence images were taken in PBS. Scale bars are 100 μm. B) Quantification of corrected total cell fluorescence (CTCF). Average fluorescence intensities were quantified by ImageJ (cell counts are > 30 for each group from three separate wells). The error bars represent the standard deviation between repeats ($n = 3$).

much higher than the other treatment groups, which demonstrated that **AAN-PTC** could deliver H_2S to the cells (Figure 4B).

We performed a similar control study in healthy H9C2 cardiomyocytes, which do not overexpress legumain. All three PHDCs showed signals on par with the small background fluorescence (Figure S14), indicating that the PHDCs in the absence of legumain could not generate

substantial amounts of H_2S. Thus, the collective in vitro results revealed that the presence of the legumain-cleavable AAN sequence is essential for H_2S release in C6 cells, and that **AAN-PTC** efficiently delivers H_2S to C6 cells at levels comparable to the instantaneous H_2S donor Na_2S.

Preparation of PHDC-Fe^{2+} Complex

We next prepared several formulations of the PHDC-Fe^{2+} complex **AAN-PTC–Fe^{2+}** by mixing different ratios of **AAN-PTC** and $FeCl_2$ in 10 mM phosphate buffer (pH 7.4). UV/Vis spectroscopy was then used to examine binding between **AAN-PTC** and Fe^{2+} (Figure S15). There was no absorbance observed for the $FeCl_2$ solution in the range of 200–400 nm, while a small peak at 250 nm appeared for the **AAN-PTC** solution. A distinct increase of the peak at 250 nm was observed with increasing amounts of $FeCl_2$ solution added to form the complex, which corresponds to the binding effect between the PHDC and Fe^{2+}. We also evaluated H_2S release from the **AAN-PTC–Fe^{2+}** complex, and it had a nearly identical profile to **AAN-PTC** alone with no precipitate formation (Figure S12C and D), consistent with good solubility of FeS at pH 5.0.[11,39]

To further investigate the binding affinity between PHDC **AAN-PTC** and Fe^{2+} in the **AAN-PTC–Fe^{2+}** complex, isothermal titration calorimetry (ITC) was performed to determine a full thermodynamic profile (ΔG, ΔH, ΔS, K_a, and binding stoichiometry) of the interaction.[40] First, control experiments (Fe^{2+} into buffer, and buffer into PHDC solution) were conducted to subtract any observed heat change that was not the direct result of PHDC-Fe^{2+} binding (Figure S16). Next, we titrated a solution of Fe^{2+} into the **AAN-PTC** solution. The ITC thermogram of the **AAN-PTC–Fe^{2+}** interaction indicated exothermic binding (Figure 5A). We then conducted a nonlinear least-squares curve fitting of the data (Figure 5B), and the fitted curve revealed a binding stoichiometry (N) of 0.95, consistent with binding of two monoanionic Glu residues to each Fe^{2+} cation. The detailed data can be seen in Table S1.

In Vitro Cytotoxicity of the PHDC-Fe^{2+} Complexes

Finally, to test our hypothesis that legumain-triggered release of H_2S, co-delivered with Fe^{2+}, can selectively kill glioma cells, we treated C6 glioma cells in vitro with the **AAN-PTC–Fe^{2+}** complex. In these experiments, cultured C6 cells were treated with either the **AAN-PTC–Fe^{2+}** complex, $FeCl_2$ alone, or **AAN-PTC** alone (all at 200 μM). Control PHDC–Fe^{2+} complexes **AAQ-PTC–Fe^{2+}** and **AAN-PC–Fe^{2+}** were also applied as a comparison with the **AAN-PTC–Fe^{2+}** complex. Finally, temozolomide (TMZ), a first-line clinical treatment for glioma,[41] was used as a positive control. Cells were treated for 24 h then imaged with live and dead stains. We also quantified cell viability via metabolic activity using the CCK-8 dye.

A high number of live cells and very few dead cells, similar to that in the untreated blank, were observed upon

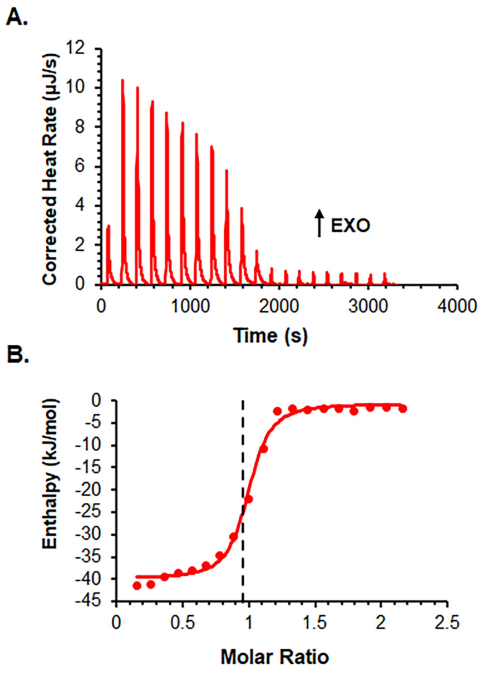

Figure 5. A) ITC thermogram of the **AAN-PTC–Fe^{2+}** titration. $FeCl_2$ solution (10 mM) was titrated into **AAN-PTC** solution (1 mM) at 298 K. B) ITC titration curve of **AAN-PTC–Fe^{2+}** titration, the red solid line is the nonlinear least-squares fitted curve, and the dashed line at 0.95 indicates the binding stoichiometry (N).

incubation with $FeCl_2$ only or **AAN-PTC** only, implying that neither H_2S nor Fe^{2+} could directly kill C6 cells (Figure 6A, rows 1–3). Similarly, neither of the control PHDC–Fe^{2+} complexes, **AAQ-PTC–Fe^{2+}** nor **AAN-PC–Fe^{2+}**, showed significant toxicity (Figure 6A, rows 4 and 5). In contrast, treatment with **AAN-PTC–Fe^{2+}** revealed a significant number of dead cells (Figure 6A, row 6), about 50 % of the total population. In a comparison treatment group, TMZ showed a similar live/dead ratio (Figure 6A, row 7), but a drug concentration of 1 mM was needed to kill approximately 50 % of cells. These live/dead imaging studies agreed with cell viability studies using the CCK-8 cell viability assay (Figure 6B). Cell viability studies on various additional control groups, including the control PHDCs without Fe^{2+}, showed no toxicity to both H9C2 and C6 cells (Figure S13A, B). Critically, none of the PHDC–Fe^{2+} complexes were toxic to H9C2 cardiomyocytes (Figure S13C). In sum, these cell viability studies confirmed the importance of the coexistence of Fe^{2+} and legumain-triggered H_2S release to kill C6 cancer cells while also demonstrating no cytotoxicity toward healthy cardiomyocytes.

To further evaluate if the PHDC–Fe^{2+} complex **AAN-PTC–Fe^{2+}** entered the cells, we examined its cellular uptake by using inductively coupled plasma mass spectrometry (ICP-MS) (Figure S14). In these experiments, C6 cells were treated for 24 h with **AAN-PTC–Fe^{2+}** at various concentrations (50, 100, 200 μM with a PHDC to Fe^{2+} ratio of 1:1 in all cases), then washed, removed from the plate with trypsin, and lysed with Triton-X-100 in a 1:1 sulfuric acid and nitric acid solution. Untreated cells were also collected

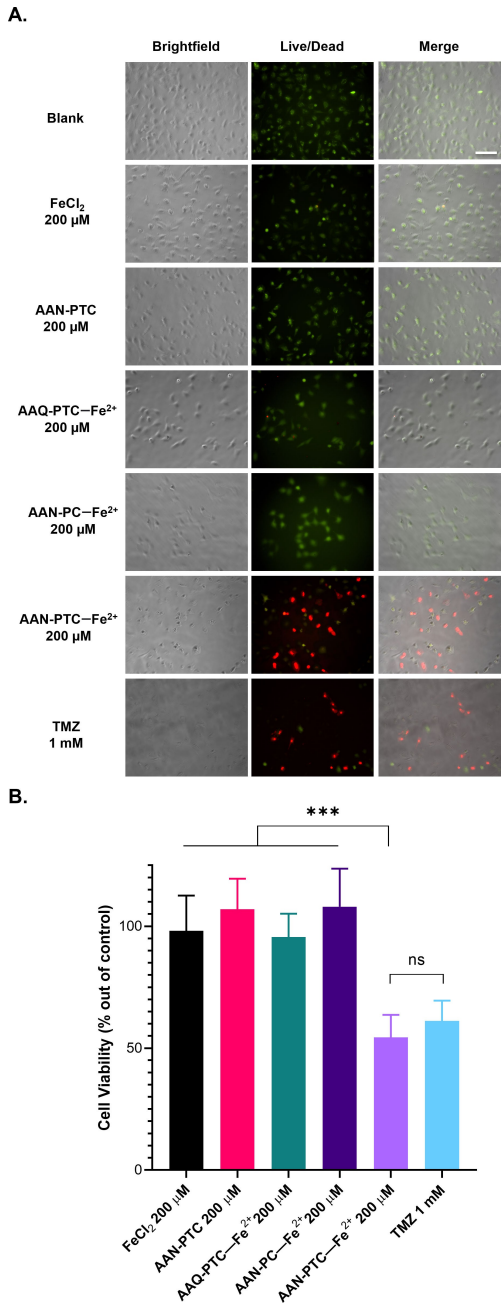

Figure 6. A) Representative bright field, live/dead, and merged images of C6 glioma cells treated with PBS buffer (blank), $FeCl_2$ (200 μM), **AAN-PTC** (with cleavable site and H_2S donor but without Fe^{2+} complexed, 200 μM), **AAQ-PTC–Fe^{2+}** (with H_2S donor but no cleavable site, 200 μM), **AAN-PC–Fe^{2+}** (with cleavable site but no H_2S donor, 200 μM), **AAN-PTC–Fe^{2+}** (with cleavable site and H_2S donor, 200 μM), and TMZ (1 mM) for 24 h post-seeding. Live/dead staining (calcein-AM and ethidium-Br) and subsequent fluorescence microscopy were performed to visualize cell viability. The scale bars represent 100 μm. Magnification = 20·x B) CCK-8 cell viability data for the same treatment groups. Error bars represent the standard deviation over three independent experiments with five replicates per experiment ($n = 3$). *** indicates $p < 0.001$ among indicated treatment groups. Group comparisons are indicated as determined by a one-way analysis of variance (ANOVA) with a Student–Newman–Keuls comparisons post hoc test.

and lysed to determine background Fe levels. Total amounts of Fe in the recovered cells were determined in triplicate by ICP-MS, subtracting background levels of iron from the control cells to determine the total amounts of Fe that were internalized (Figure S17). Results showed that cellular uptake increased with increasing concentration of **AAN-PTC–Fe^{2+}**; for example, cellular uptake of 200 μM **AAN-PTC–Fe^{2+}** was 42 %, about 1.5-fold higher than that of 50 μM (≈28 %). Along with the H_2S imaging studies (Figure 4), and the cell viability results (Figure 6), the ICP-MS data suggest significant cellular internalization of **AAN-PTC–Fe^{2+}**.

Finally, to evaluate whether the observed cell-killing effect was indeed due to increased oxidative stress, we measured ROS levels inside C6 cells upon treatment with PHDC–Fe^{2+} complexes. In these experiments, we treated cells with the three PHDC–Fe^{2+} complexes for 3 h and then added dihydroethidium (DHE) as an ROS-sensing fluorescent probe, similar to previous studies on PHDCs.[42,43] High intracellular ROS levels are evidenced in these experiments by significant red fluorescence (Figure 7A).

The blank control group (C6 cells without any treatment, Figure 7A row 1) exhibited a low red fluorescent signal, which can be explained by a relatively low level of ROS naturally generated in the cells due to CAT activity. However, after treatment with **AAN-PTC–Fe^{2+}**, a vast increase in the intensity of the red fluorescence signal was observed (Figure 7A, row 2), implying that ROS had accumulated in the cells. In contrast, in cells treated with either **AAQ-PTC–Fe^{2+}** or **AAN-PC–Fe^{2+}**, the fluorescent intensity resembled the blank control (Figure 7A, rows 3 and 4), indicating that the control PHDC–Fe^{2+} complexes did not influence ROS levels in the C6 cells. We also evaluated ROS levels using DHE in cells treated with $FeCl_2$ (Figure 7A, row 5), which showed low levels similar to the control PHDC–Fe^{2+} complexes, and **AAN-PTC** alone (Figure 7A, row 6), which showed increased ROS levels above the untreated blank but lower than the **AAN-PTC–Fe^{2+}** treatment group. This result is consistent with the inhibition of CAT by H_2S. Similarly, studies on CAT activity in C6 cells with various treatments showed reduced CAT activity in cells treated with **AAN-PTC** and even further reduced activity in cells treated with **AAN-PTC–Fe^{2+}** (Figure S18). Collectively, these results are consistent with the cell viability assays and live/dead fluorescence studies, supporting our hypothesis that the Fenton reaction, induced by Fe^{2+} and enhanced by inhibition of CAT by H_2S, leads to cell killing via a significant increase in ROS levels. This phenomenon indicates that both H_2S and Fe^{2+} are essential to kill C6 cells, as well as the existence of the ubiquitous enzyme CA and overexpressed legumain.

Conclusion

In summary, we report for the first time a dual-responsive, peptide-based Fe complex, **AAN-PTC–Fe^{2+}**, which releases H_2S in C6 glioma cells in response to overexpressed legumain and ubiquitous carbonic anhydrase. The legumain-

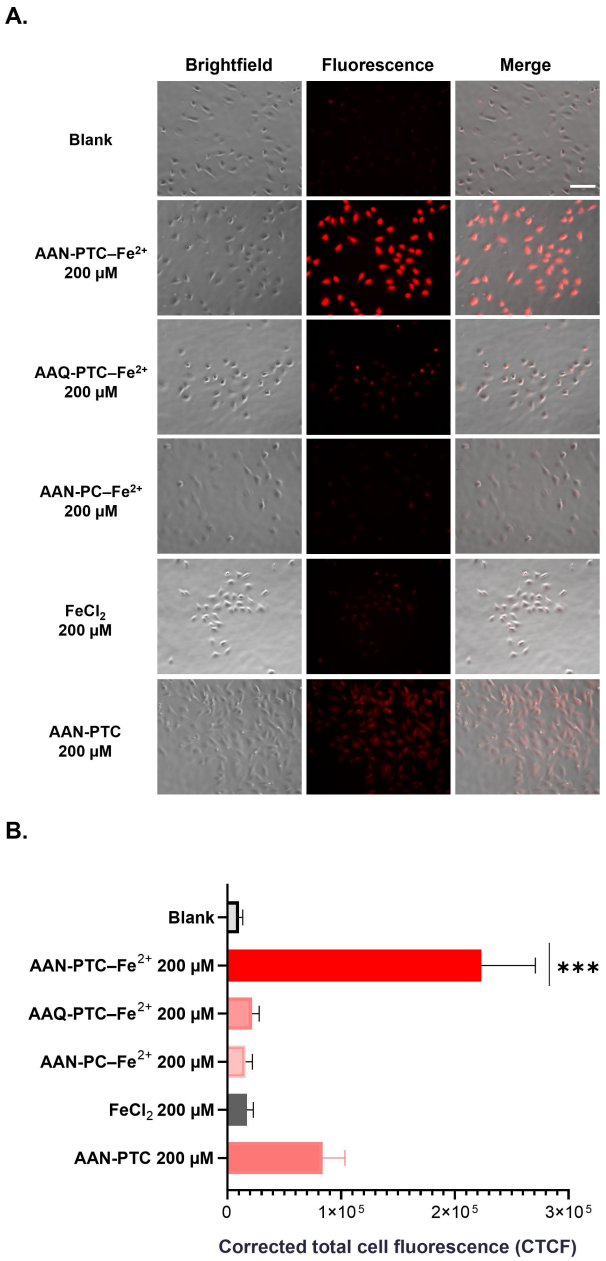

Figure 7. A) Bright field, fluorescence, and merged images showing fluorescence in C6 rat glioma cells preincubated with either PBS (blank), **AAN-PTC–Fe^{2+}** (with cleavable site and H_2S donor, 200 μM), **AAQ-PTC–Fe^{2+}** (with H_2S donor but no cleavable site, 200 μM), **AAN-PC–Fe^{2+}** (with cleavable site but no H_2S donor, 200 μM), $FeCl_2$ (200 μM), and **AAN–PTC** (with cleavable site and H_2S donor but no Fe^{2+}, 200 μM) for 3 h. After treatment, cells were incubated with ROS probe DHE (10 μM) for 30 min, washed, and imaged in DPBS by bright-field and fluorescence microscopy. Scale bar is 100 μm. B) Corrected total cell fluorescence (CTCF) quantification for the same treatment groups. Average fluorescence intensities were quantified using ImageJ (cell counts are >30 for each group from three separate wells). The error bars represent the standard deviation among repeats ($n=3$). *** indicates $p<0.001$ for a comparison of **AAN-PTC–Fe^{2+}** versus all other groups, which was determined by a one-way analysis of variance (ANOVA) with a Student-Newman-Keuls comparisons post hoc test.

responsive motif AAN was first conjugated to a thionocarbonate that could be triggered upon cleavage of the AAN unit to form COS and then H_2S, an inhibitor of the H_2O_2-detoxifying enzyme CAT. This PHDC was further complexed with Fe^{2+} to promote ROS production by a Fenton reaction. The **AAN-PTC–Fe^{2+}** complex showed significant H_2S release in the C6 glioma cell line, which overexpresses legumain, compared with control PHDCs that either lacked the AAN sequence or the ability to generate H_2S. **AAN-PTC–Fe^{2+}** generated high levels of intracellular ROS that killed C6 cells even better than the first-line chemotherapy drug TMZ. These results demonstrate the pro-oxidant effects of H_2S in this system and highlight the "double-faced" nature of this gasotransmitter, which can also serve as an antioxidant, a topic of current debate.[44] Finally, the **AAN-PTC–Fe^{2+}** complex showed no toxicity toward H9C2 cardiomyocytes, which is critical because cardiotoxicity is the dose-limiting side effect of many chemotherapeutics. These results collectively highlight the potential of **AAN-PTC–Fe^{2+}** in precise glioma treatments, demonstrating the utility of CDT combined with cancer cell-specific delivery of H_2S to inhibit CAT and increase ROS levels. More broadly, these studies show how the gasotransmitter H_2S can enhance existing therapies through targeted delivery strategies.

Acknowledgements

This work was supported by the National Institutes of Health (R01GM123508). The TOC graphic was created with BioRender.com. We thank Professor Andrew Lowell for the use of the plate reader, Professor Rafael Davalos, Dr. Anand Vadlamani, and Barath Udayasuryan for assistance with the C6 glioma cell line; Dr. Willian Keith Ray for assistance with MALDI-TOF experiments; Dr. Jeffery L. Parks for ICP-MS analyses; Professor Emily Mevers and Dr. Carla Menegatti for assistance with LC–MS experiments; and Connor Gallagher for providing helpful information on ITC. Finally, we thank Sarah Swilley, Clark Vu and Dr. Rajnish Kumar for critical reading of the manuscript, and Zhao Li and Kearsley M. Dillon for helpful suggestions.

Conflict of Interest

The authors declare no conflict of interest.

Data Availability Statement

The data that support the findings of this study are available in the Supporting Information of this article.

Keywords: Cancer · Drug Delivery · Gasotransmitter · Iron · Prodrugs

[1] J. Wang, J. Yi, *Cancer Biol. Ther.* **2008**, *7*, 1875–1884.

[2] C. Zhang, W. Bu, D. Ni, S. Zhang, Q. Li, Z. Yao, J. Zhang, H. Yao, Z. Wang, J. Shi, *Angew. Chem. Int. Ed.* **2016**, *55*, 2101–2106.
[3] X. Li, Q. Zhou, A. A.-W. M. M. Japir, D. Dutta, N. Lu, Z. Ge, *ACS Nano* **2022**, *16*, 14982–14999.
[4] P. Zhao, H. Li, W. Bu, *Angew. Chem. Int. Ed.* **2023**, *62*, e202210415.
[5] X. Wang, X. Zhong, Z. Liu, L. Cheng, *Nano Today* **2020**, *35*, 100946.
[6] X. Ma, D. Deng, W. Chen in *Enzyme Inhibitors and Activators* (Ed.: M. Senturk), IntechOpen, **2017**, pp. 207–224.
[7] L. R. Benetti, D. Campos, S. A. Gurgueira, A. E. Vercesi, C. E. V. Guedes, K. L. Santos, J. L. Wallace, S. A. Teixeira, J. Florenzano, S. K. P. Costa, M. N. Muscará, H. H. A. Ferreira, *Eur. J. Pharmacol.* **2013**, *698*, 463–469.
[8] L. Fu, Z. Wei, K. Hu, L. Hu, Y. Li, X. Chen, Z. Han, G. Yao, H. Zhang, *J. Microbiol.* **2018**, *56*, 238–245.
[9] J. Li, C. Shi, X. Wang, C. Liu, X. Ding, P. Ma, X. Wang, H. Jia, *Plant Physiol. Biochem.* **2020**, *156*, 257–266.
[10] Q. Tian, L. An, Q. Tian, J. Lin, S. Yang, *Theranostics* **2020**, *10*, 4101–4115.
[11] C. Xie, D. Cen, Z. Ren, Y. Wang, Y. Wu, X. Li, G. Han, X. Cai, *Adv. Sci.* **2020**, *7*, 1903512.
[12] K. Abe, H. Kimura, *J. Neurosci.* **1996**, *16*, 1066–1071.
[13] D. Wu, W. Si, M. Wang, S. Lv, A. Ji, Y. Li, *Nitric Oxide* **2015**, *50*, 38–45.
[14] K. Kashfi, *Biochem. Pharmacol.* **2018**, *149*, 205–223.
[15] S. Bao, Q. Wu, S. Sathornsumetee, Y. Hao, Z. Li, A. B. Hjelmeland, Q. Shi, R. E. McLendon, D. D. Bigner, J. N. Rich, *Cancer Res.* **2006**, *66*, 7843–7848.
[16] K. D. Miller, Q. T. Ostrom, C. Kruchko, N. Patil, T. Tihan, G. Cioffi, H. E. Fuchs, K. A. Waite, A. Jemal, R. L. Siegel, J. S. Barnholtz-Sloan, *Ca-Cancer J. Clin.* **2021**, *71*, 381–406.
[17] M. Saleh, S. A. Stacker, A. F. Wilks, *Cancer Res.* **1996**, *56*, 393–401.
[18] K. Karimipour, J. Keyvan Rad, S. Shirvalilou, S. Khoei, A. R. Mahdavian, *Colloids Surf. B* **2021**, *203*, 111731.
[19] A. G. K. Ferreira, H. Biasibetti-Brendler, D. S. V. Sidegum, S. O. Loureiro, F. Figueiró, A. T. S. Wyse, *Neurotoxic. Res.* **2021**, *39*, 327–334.
[20] B. Goel, A. Sharma, N. Tripathi, N. Bhardwaj, B. Sahu, G. Kaur, B. Singh, S. K. Jain, *Nat. Prod. Res.* **2021**, *35*, 5489–5492.
[21] S. Wongkularb, T. Limboonreung, P. Tuchinda, S. Chongthammakun, *In Vitro Cell. Dev. Biol. Anim.* **2022**, *58*, 29–36.
[22] M. Ersoz, A. Erdemir, S. Derman, T. Arasoglu, B. Mansuroglu, *Pharm. Dev. Technol.* **2020**, *25*, 757–766.
[23] R. Kunjumon, G. Viswanathan, S. Baby, *Carbohydr. Polym. Technol. Appl.* **2021**, *2*, 100106.
[24] Y. Zhen, G. Chunlei, S. Wenzhi, Z. Shuangtao, L. Na, W. Rongrong, L. Xiaohe, N. Haiying, L. Dehong, J. Shan, T. Xiaoyue, X. Rong, *Sci. Rep.* **2015**, *5*, 16599.
[25] J. Zhan, J. Zhong, W. Ma, S. Ma, Y. Wang, Z. Yu, Y. Cai, W. Huang, *Chem. Commun.* **2020**, *56*, 6957–6960.
[26] C. R. Powell, K. M. Dillon, J. B. Matson, *Biochem. Pharmacol.* **2018**, *149*, 110–123.
[27] X. Ni, S. S. Kelly, S. Xu, M. Xian, *Acc. Chem. Res.* **2021**, *54*, 3968–3978.
[28] E. Magli, E. Perissutti, V. Santagada, G. Caliendo, A. Corvino, G. Esposito, G. Esposito, F. Fiorino, M. Migliaccio, A. Scognamiglio, B. Severino, R. Sparaco, F. Frecentese, *Biomol. Eng.* **2021**, *11*, 1899.
[29] C. M. Levinn, M. M. Cerda, M. D. Pluth, *Antioxid. Redox Signaling* **2020**, *32*, 96–109.
[30] C. M. Levinn, M. M. Cerda, M. D. Pluth, *Acc. Chem. Res.* **2019**, *52*, 2723–2731.
[31] K. Kaur, P. Enders, Y. Zhu, A. F. Bratton, C. R. Powell, K. Kashfi, J. B. Matson, *Chem. Commun.* **2021**, *57*, 5522–5525.
[32] M. M. Cerda, J. L. Mancuso, E. J. Mullen, C. H. Hendon, M. D. Pluth, *Chem. Eur. J.* **2020**, *26*, 5374–5380.
[33] P. Chauhan, P. Bora, G. Ravikumar, S. Jos, H. Chakrapani, *Org. Lett.* **2017**, *19*, 62–65.
[34] Y. Zhao, A. K. Steiger, M. D. Pluth, *Chem. Commun.* **2018**, *54*, 4951–4954.
[35] C. R. Powell, J. C. Foster, B. Okyere, M. H. Theus, J. B. Matson, *J. Am. Chem. Soc.* **2016**, *138*, 13477–13480.
[36] Y. Wang, K. Kaur, S. J. Scannelli, R. Bitton, J. B. Matson, *J. Am. Chem. Soc.* **2018**, *140*, 14945–14951.
[37] E. Dall, J. C. Fegg, P. Briza, H. Brandstetter, *Angew. Chem. Int. Ed.* **2015**, *54*, 2917–2921.
[38] B. Peng, W. Chen, C. Liu, E. W. Rosser, A. Pacheco, Y. Zhao, H. C. Aguilar, M. Xian, *Chem. Eur. J.* **2014**, *20*, 1010–1016.
[39] D. Rickard, *Geochim. Cosmochim. Acta* **2006**, *70*, 5779–5789.
[40] W. R. Archer, M. D. Schulz, *Soft Matter* **2020**, *16*, 8760–8774.
[41] M. Li, R. Liang Fei, X. Wang, Q. Mao, Y. Liu Hui, *Oncol. Lett.* **2017**, *14*, 6597–6603.
[42] Y. Wang, Z. Li, Y. Shmidov, R. J. Carrazzone, R. Bitton, J. B. Matson, *J. Am. Chem. Soc.* **2020**, *142*, 20058–20065.
[43] Y. Wang, K. M. Dillon, Z. Li, E. W. Winckler, J. B. Matson, *Angew. Chem. Int. Ed.* **2020**, *59*, 16698–16704.
[44] B. Olas in *Advances in Clinical Chemistry* (Ed.: G. S. Makowski), Elsevier, Amsterdam, **2017**, pp. 187–196.

Manuscript received: February 14, 2023
Version of record online: April 20, 2023